Report

Current Biology

Bi-directional Control of Walking Behavior by Horizontal Optic Flow Sensors

Graphical Abstract

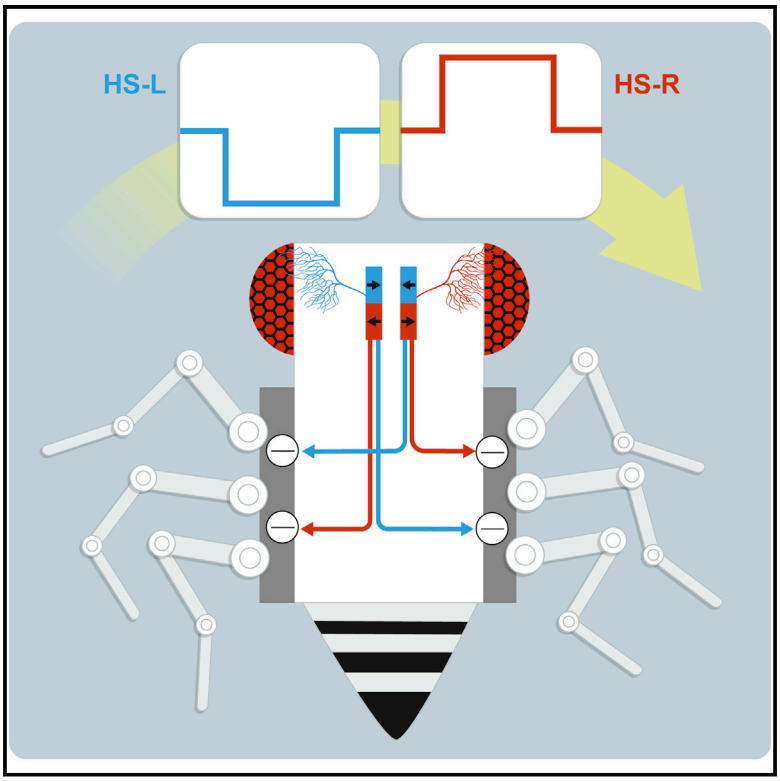

Authors

Christian Busch, Alexander Borst, Alex S. Mauss

Correspondence

amauss@neuro.mpg.de

In Brief

Busch et al. study the behavioral effects of manipulating optic flow-sensing HS cells in tethered walking *Drosophila*. Both de- and hyperpolarization elicit turning syndirectional with the mimicked visual motion. Therefore, two steering signals are encoded in the HS cell-response sign, likely mediating the fly's tendency to follow a rotating pattern.

Highlights

- Horizontal optic flow detectors (HS cells) affect turning in walking flies
- De- and hyperpolarization evoke opposite turning
- Both signals negatively influence walking speed
- HS cells thus mediate bi-directional turning via asymmetric deceleration

Busch et al., 2018, Current Biology *28*, 1–9
December 17, 2018
https://doi.org/10.1016/j.cub.2018.11.010

CellPress

Please cite this article in press as: Busch et al., Bi-directional Control of Walking Behavior by Horizontal Optic Flow Sensors, Current Biology (2018), https://doi.org/10.1016/j.cub.2018.11.010

Current Biology
Report

Bi-directional Control of Walking Behavior by Horizontal Optic Flow Sensors

Christian Busch,[1] Alexander Borst,[1] and Alex S. Mauss[1,2,*]
[1]Circuits - Computation - Models, Max Planck Institute of Neurobiology, Am Klopferspitz 18, Martinsried 82152, Germany
[2]Lead Contact
*Correspondence: amauss@neuro.mpg.de
https://doi.org/10.1016/j.cub.2018.11.010

SUMMARY

Moving animals experience constant sensory feedback, such as panoramic image shifts on the retina, termed optic flow. Underlying neuronal signals are thought to be important for exploratory behavior by signaling unintended course deviations and by providing spatial information about the environment [1, 2]. Particularly in insects, the encoding of self-motion-related optic flow is well understood [1–5]. However, a gap remains in understanding how the associated neuronal activity controls locomotor trajectories. In flies, visual projection neurons belonging to two groups encode panoramic horizontal motion: horizontal system (HS) cells respond with depolarization to front-to-back motion and hyperpolarization to the opposite direction [6, 7], and other neurons have the mirror-symmetrical response profile [6, 8, 9]. With primarily monocular sensitivity, the neurons' responses are ambiguous for different rotational and translational self-movement components. Such ambiguities can be greatly reduced by combining signals from both eyes [10–12] to determine turning and movement speed [13–16]. Here, we explore the underlying functional logic by optogenetic HS cell manipulation in tethered walking *Drosophila*. We show that de- and hyperpolarization evoke opposite turning behavior, indicating that both direction-selective signals are transmitted to descending pathways for course control. Further experiments reveal a negative effect of bilaterally symmetric de- and hyperpolarization on walking velocity. Our results are therefore consistent with a functional architecture in which the HS cells' membrane potential influences walking behavior bi-directionally via two decelerating pathways.

RESULTS

In the fly optic lobe, optic flow-sensing tangential cells can be found in the lobula plate, four synapses downstream of photoreceptors (Figure 1A). They receive excitatory input from local motion detectors, T4/T5 cells [17, 18], and inhibitory input from bi-stratified relay neurons, termed LPi [19] (Figure 1B). T4/T5 terminals are sorted according to their directional preference into four layers such that opposite directions of motion are represented side by side [18, 21]. As a consequence, predominantly mono-stratified tangential cells respond with depolarization to motion along their preferred direction (PD) and hyperpolarization to motion along the opposite or null direction (ND) motion [6, 7]. Because tangential cells in layer 1 and 2 exhibit mirror-symmetrical motion preferences, any horizontal motion (front-to-back or back-to-front) is simultaneously represented in layer 1 and 2 cells by responses with opposite signs (Figure 1C). Here, we explore how such signals control walking behavior by conceptualizing a fly as a Braitenberg vehicle [20], with left and right motors representing the fly walking apparatus (Figures 1D–1G). Each horizontal motion detector comprises a PD and an ND channel that convey direction-selective signals. Those are negatively or positively connected to left and right motors such that the connectivity supports turning syndirectional with horizontal motion. For instance, activating front-to-back-selective signals on the left side can either accelerate the right motor (Figures 1D and 1F) or decelerate the left motor (Figures 1E and 1G) to mediate syndirectional leftward turning. We ask (1) whether only PD signals (carried by depolarizations) are conveyed to downstream neurons to affect locomotor behavior (Figures 1D and 1E) or whether ND signals (carried by hyperpolarizations) also contribute (Figures 1F and 1G) and (2) whether the signals act positively (Figures 1D and 1F) or negatively (Figures 1E and 1G) on the propulsive forces underlying walking [13].

Visual and Optogenetic Control over Horizontal System Cell Activity

To address the functional logic underlying steering by horizontal PD and ND signals, we expressed two different light-activatable channels in horizontal system (HS) cells, which allowed us to induce PD- and ND-like activities: depolarizing cation-conducting ReaChR [22, 23] and hyperpolarizing chloride-conducting GtACR1 [24, 25]. We characterized visual and optogenetic effects of illumination on the HS cells' membrane potential by *in vivo* patch-clamp recordings (Figure 2A). HS cells in control flies (without expression) exhibited depolarizing ON and OFF transients and subtle tonic depolarization in response to 565 nm light, indicating that the light pulse delivered through the microscope is visually perceived by flies (Figure 2B, black trace). This is expected, given the large dynamic range in which visual systems operate. The responses of ReaChR- and GtACR1-expressing HS cells were markedly different in that

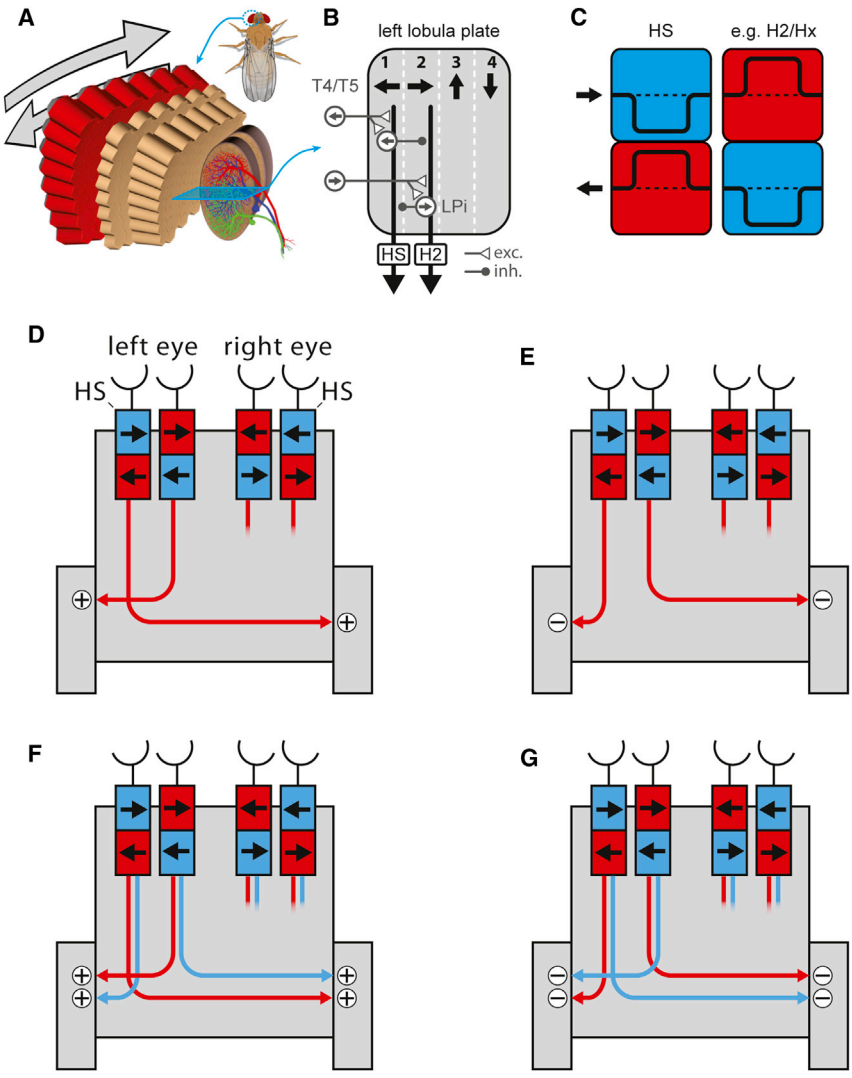

Figure 1. Course Control by Horizontal Optic Flow Sensors

(A) The fly optic lobe (left side) in schematic form, with HS cells of the lobula plate shown.

(B) The functional organization of the lobula plate. T4/T5 terminals provide excitatory inputs [17], sorted into 4 layers according to their directional preference [18]. Mono-stratified tangential cells are thus excited for motion in their preferred direction (PD). Opposite, null direction (ND) inhibition presumably arises by sign-inverting feedforward connections across motion-opponent layers via LPi neurons, as shown for layer 4 tangential cells [19]. Note that the focus here lies on HS cells, with H2 given as one layer 2 example.

(C) Tangential cells of layer 1 (HS cells) and 2 (e.g., H2 or Hx cells) exhibit mirror-symmetrical PD (red) and ND (blue) motion responses.

(D–G) Different versions of a fly conceived as a Braitenberg vehicle [20]. Inputs represent the mirror-symmetrical layer 1 (HS) and 2 lobula plate tangential cells each comprising a PD (red) and ND channel (blue). Signals carried by these channels impinge on left and right motors with positive (+) or negative (–) effect but in all cases supporting turning syndirectional with the perceived horizontal motion direction.

(D and E) Only PD signals are connected to motors, either with a positive (D) or negative (E) effect.

(F and G) Additional ND signals are connected, again either with a positive (F) or negative (G) effect.

they tonically de- and hyperpolarized, respectively, with amplitudes depending on log light intensity with a sigmoidal relationship (Figures 2B and 2C). Above 10 and 2.5 $\mu W/mm^2$, respectively, visual ON and OFF transients were masked by these robust responses. Apart from the sign, both channels mediated large maximal potential changes of comparable amplitudes (~20 mV). However, GtACR1 responses were slightly more light sensitive (50% response at 6.5 $\mu W/mm^2$ for GtACR1 as opposed to 24.8 $\mu W/mm^2$ for ReaChR; Figure 2C). Furthermore, imparted HS cell potential changes differed in the time course for the two channels: for responses of comparable amplitudes, ReaChR-mediated depolarization had ON and OFF time constants of 31 and 172 ms, respectively, and GtACR1-mediated hyperpolarization exhibited ON and OFF time constants of 9 and 609 ms (Figures 2B and S1).

We then combined optogenetic HS cell manipulation with visual stimulation (Figure 2D). A preferred direction motion stimulus on its own depolarized HS cells and a null direction motion stimulus led to hyperpolarization. In control flies, with increasing optogenetic light intensity, visually mediated responses were only affected at high illumination intensities, presumably due to photoreceptor activation, leading to a reduced perceived grating contrast. This shows that dimmer optogenetic illumination leaves visual photoreceptor signals intact. Repeating this protocol in flies expressing ReaChR and GtACR1 in the recorded HS cells led to robust potential changes superimposed on the visual response. PD depolarization was enhanced by ReaChR and reduced by GtACR1 (Figures 2D and 2E). The opposite was true for visually mediated ND hyperpolarization, which was enhanced by GtACR1 and reduced by ReaChR. Therefore, ReaChR and GtACR1 are suitable tools to fast and reversibly control HS cell activity in either response direction, without compromising visual signals in photoreceptors.

Monocular HS Cell De- and Hyperpolarization Elicit Opposite Turning Responses

Next, we explored the effects of monocular HS cell activity manipulations in tethered walking flies (Figure 3A). We performed experiments with five different lines, all sharing expression of optogenetic tools in HS cells (R27B03, R24E09, R81G07, VT023749, and VT058487) [26] at various degrees of strength and selectivity. This way, we reduced the risk of misinterpreting phenotypes arising from off-target expression. Initially, we expressed ReaChR using all five driver lines and tested optomotor responses to a monocular visual stimulus moving front to back (results for one line shown in Figure 3B). Flies of three out of the five genotypes showed normal optomotor response behavior

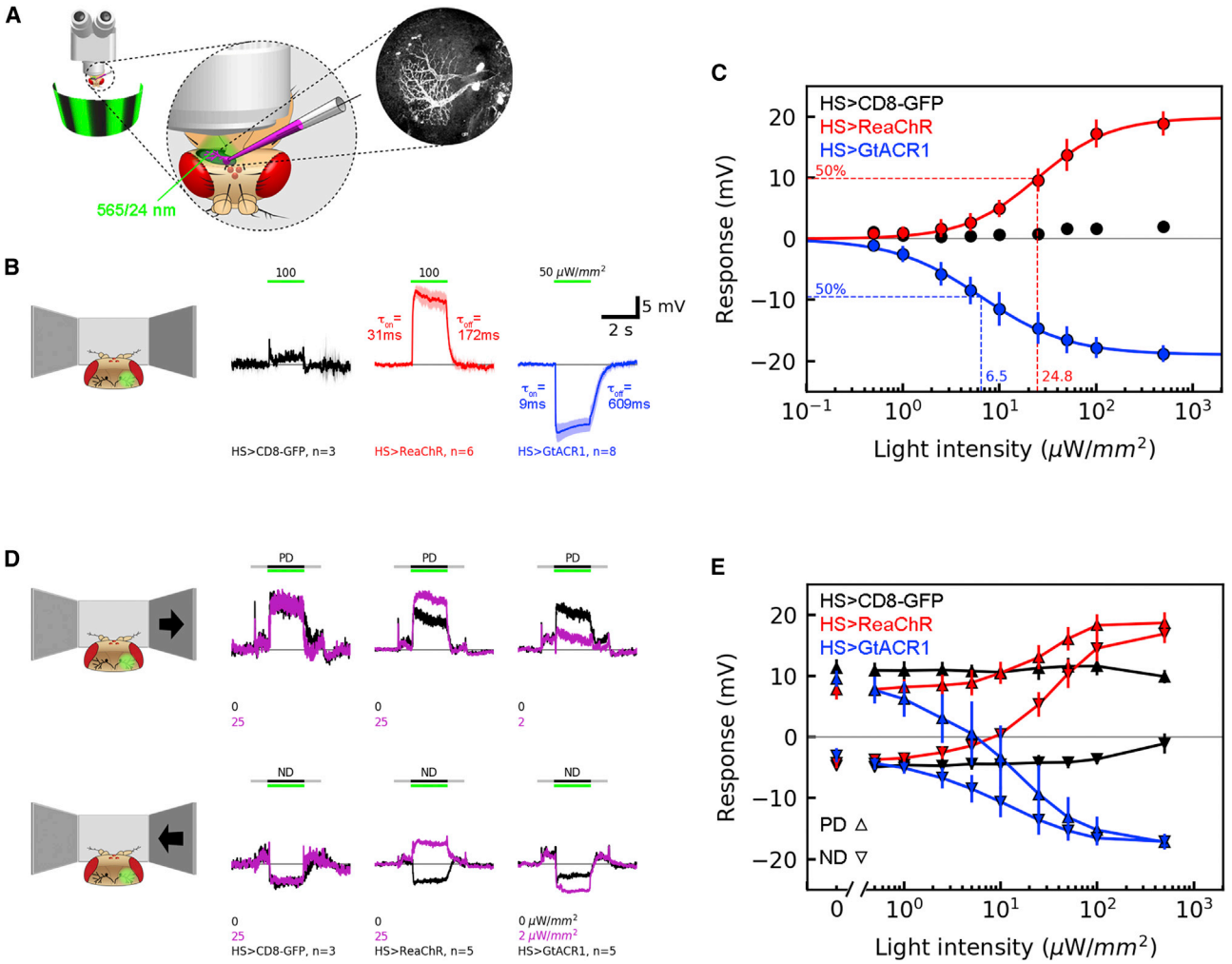

Figure 2. Optogenetic Manipulation of HS Cell Activity

(A) Illustration of recording setup. HS cell membrane potential is obtained via whole-cell patch-clamp recording. Optogenetic illumination is delivered via the microscope objective by passing light through an optical filter with 565 nm center wavelength and 24 nm bandwidth. Visual motion stimulation is provided by a light-emitting diode (LED) screen in front of the fly.

(B) HS cell recording traces averaged across trials and cells. 2 s illumination of control flies (without expression) has modest and mostly transient visual effects on membrane potential. In contrast, ReaChR- and GtACR1-expressing HS cells exhibit robust de- and hyperpolarization, respectively. To assess optogenetic response dynamics, an exponential decay function was fit to response onset and offset to obtain the time constants τ_{ON} and τ_{OFF} (see STAR Methods and Figure S1).

(C) Quantification of experiment shown in (B) for nine light intensities. Data are presented as baseline subtracted light responses. A sigmoid function (see STAR Methods) was fit to the ReaChR and GtACR1 data points and used to determine the light intensity for evoking 50% of the maximal response.

(D) Same as (B) but with simultaneous PD and ND visual motion stimulation. 1 s before and after grating motion, the grating was stationary (gray bars), causing ON and OFF transients upon appearance and disappearance. Potential changes during grating motion are a combination of visual and optogenetic responses.

(E) Quantification as in (C). Note that visual responses in control flies (without expression) are compromised only at the highest light intensity (500 $\mu W/mm^2$; close to optogenetic channel saturation), due to photoreceptor activation presumably reducing the perceived visual contrast.

Data are presented as mean ± SD (omitted in D) across 2 trials and n flies. See also Figure S1.

(R27B03, VT023749, and VT058487). However, flies of two genotypes exhibited impaired optomotor responses, indicating unspecific visual or motor defects, and were therefore excluded from further optogenetic experiments (R24E09 and R81G07). In the three remaining genotypes, we optogenetically depolarized HS cells on one side of the head, which evoked turning toward the side of illumination (Figures 3B–3D). This response is syndirectional with the mimicked visual motion direction (front to back) and in agreement with published literature [14], where HS axon depolarization via ATP-gated P2X2 channel activation evoked similar turning. The comparison between visual and optogenetically induced turning (Figure 3C) shows that the initial average turning response to monocular visual stimulation (dashed lines) is comparable to optogenetically induced turning. However, the dynamics are different in that visually evoked turning is tonic and optogenetic responses are more phasic in nature. Furthermore, the optogenetically induced turning response peaked at a certain illumination intensity and then

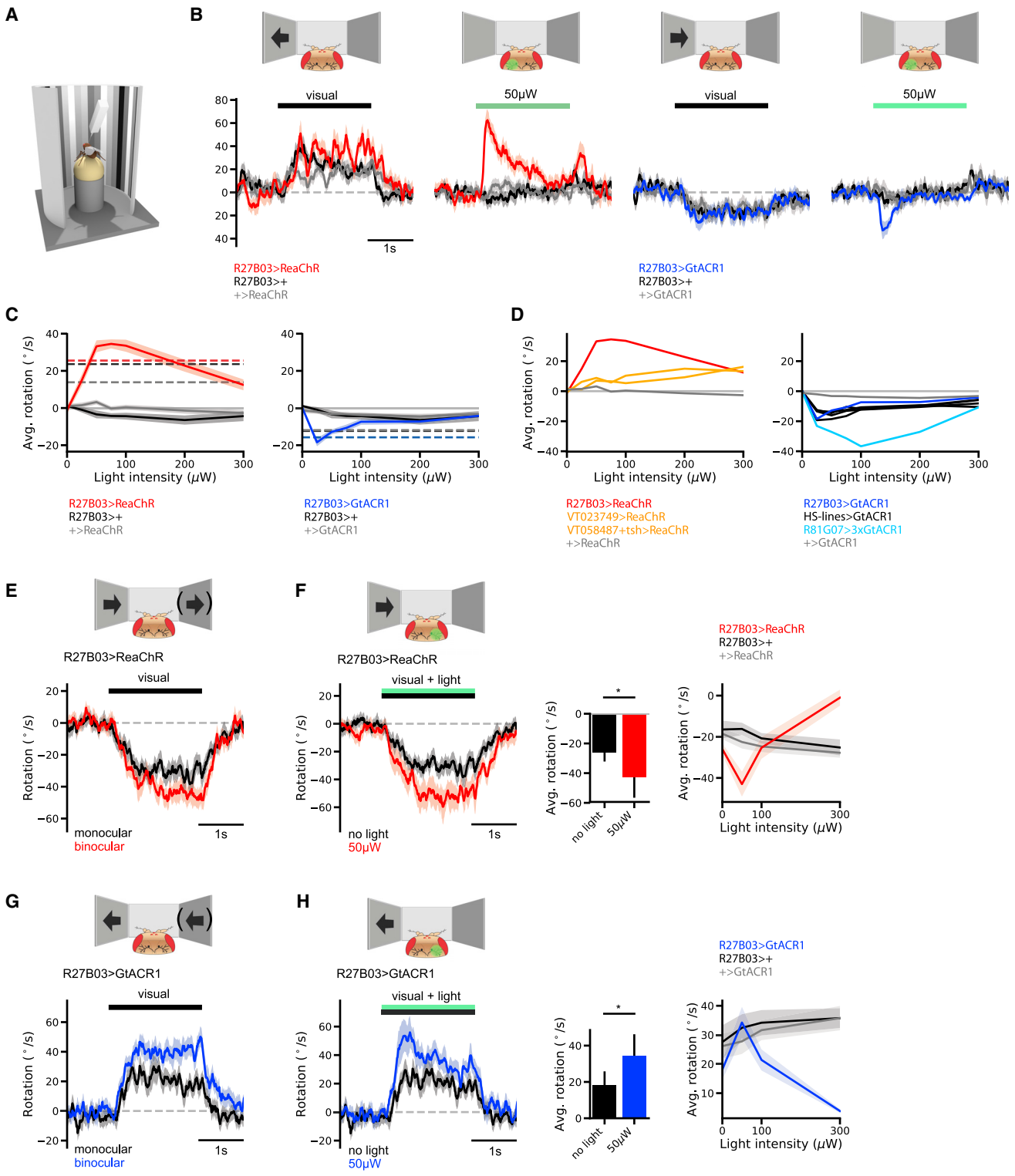

Figure 3. Visually and Optogenetically Evoked Turning Behavior

(A) Illustration of the tethered walking setup (see STAR Methods).

(B) Comparison between monocular visual and optogenetic induced turning, using ReaChR and GtACR1.

(C) Time-averaged turning responses (first second of optogenetic stimulation) of experiments shown in (B), including different light intensities. Dashed lines represent the average monocular visual turning response.

(D) Average turning responses for different driver lines (experiment as illustrated in B; plot as described in C, without visual response).

(legend continued on next page)

declined. This decline might be due to light scattering to the contralateral side [24], activating both left and right HS cells.

We performed a complementary set of experiments using GtACR1 instead of ReaChR to address the question whether HS cell hyperpolarization also affects walking behavior. All five lines expressing GtACR1 showed normal optomotor behavior to visual, monocular back-to-front stimulation; hence, no line was excluded. This time, optogenetic hyperpolarization of HS cells evoked turning in the opposite direction to what we observed during depolarization for all tested lines (Figures 3B–3D) but again syndirectional with the mimicked visual motion direction (back to front). Hence, like depolarization, monocular hyperpolarization of HS cells affects steering behavior. As for ReaChR, GtACR1-mediated turning was phasic in nature, in contrast to more tonic visually evoked responses, and had a response peak at a certain illumination intensity. We then compared expression between all driver lines using fluorescence imaging (enhanced yellow fluorescent protein [EYFP]-tagged optogenetic channels using identical microscopy settings without any amplification step via immunostaining; Figure S2). R81G07 seemed to be the most specific line. However, it mediated often weak and variable expression, sometimes in only one HS cell per hemisphere. This observation matched variable and often modest behavioral effects across flies following illumination. By increasing the expression levels using multiple copies of the optogenetic transgene (Figure S2), the optogenetic turning response could be markedly increased (Figure 3D), highlighting the importance of expression levels for assessing experimental phenotypes.

Increasing Binocular HS Cell Response Asymmetry Enhances Turning Behavior

Yaw rotation usually evokes optic flow on both eyes: front to back on one and back to front on the other side. A corresponding visual stimulus evokes turning in tethered walking flies that is increased with respect to monocular motion (Figures 3E and 3G). Thus, the question arises how the combined left and right HS cell activity affects steering. Because it is technically challenging to express ReaChR and GtACR1 in HS cells on opposite sides, we combined visual and optogenetic HS cell stimulation. To mimic a binocular rotational motion stimulus involving asymmetric left and right HS activity, we presented back-to-front motion on one side and depolarized HS cells via ReaChR on the other side. In a low-light regime, this resulted in an enhanced turning response compared to the visual stimulus alone (Figure 3F). Increasing the light intensity further reduced overall turning, likely due to light scattering to the contralateral side and activating both left and right HS cells [24]. The converse manipulation mimicking binocular rotation in the other direction—visual front-to-back motion and GtACR1-mediated hyperpolarization on the contralateral side—had equivalent enhancing effects (Figure 3H). These experiments provide further support for the notion that both de- and hyperpolarization from left and right HS cells are integrated downstream to affect turning. They also demonstrate the feasibility of selectively modulating neuronal activity in opposite directions within active visual circuits, representing a powerful experimental system for future studies.

Symmetric Binocular HS Cell Potential Changes Reduce Walking Speed

Considering a walking animal, turning can be brought about by reducing propulsive forces on the inner side of the curve and/or enhancing those on the outer side [13]. The former also reduces forward walking velocity and the latter increases it. Using flies on a tread compensator, Götz and Wenking [13] have found evidence for either, depending on the genotype and condition. However, using a tethered walking assay, Silies et al. [27] measured robust non-directional reductions in walking speed in response to both front-to-back and back-to-front motion. We revisited the effects of both binocular rotating and translating stimuli on walking speed and, in line with the latter study, obtained prominent speed reductions for all stimuli (Figures 4A, 4B, 4D, and 4E). This suggests a predominantly decelerating effect of wide-field horizontal motion detectors, such as HS cells on the motor system. Increasing motion speed of a translational stimulus (200 versus 80°/s) led to stronger deceleration, suggesting a stronger activation of the underlying pathway (Figures 4B and 4E). To probe the influence of HS cells on walking velocity, we de- and hyperpolarized HS cells on both sides simultaneously via ReaChR and GtACR1. Like the corresponding visual stimuli, both binocular manipulations led to a substantial reduction of walking speed (Figures 4B, 4C, 4E, and 4F). In summary, our results are in agreement with a functional architecture in which positive and negative HS cell signals are split into two pathways that both negatively affect left and right propulsive motor forces (Figure 1G).

DISCUSSION

Wide-field motion-sensitive neurons have been extensively studied to elucidate the mechanisms leading to motion detection and flow field selectivity [1–5, 28, 29]. In contrast, how their signals affect steering behavior has only been explored regarding the influence of depolarization on turning [14, 15]. Here, we have used recently characterized de- and hyperpolarizing optogenetic tools [22–25] to indicate further causal links between the activity of HS cells and tethered walking behavior in flies. Our results reveal two

(E) Comparison of the turning response to monocular back-to-front and binocular rotation.

(F) Left: Fly turning response to monocular back-to-front pattern motion with and without simultaneous contralateral optogenetic HS cell activation. (Middle) Quantification of the experiment. (Right) Average rotation response of R27B03 > ReaChR compared to controls for different light intensities.

(G) Comparison of the turning response to monocular front-to-back and binocular rotation.

(H) Left: Fly turning response to monocular front-to-back pattern motion with and without simultaneous contralateral optogenetic HS cell hyperpolarization. (Middle) Quantification of the experiment. (Right) Average rotation response of R27B03 > GtACR1 compared to controls for different light intensities.

Traces represent the mean ± SEM. Symmetric experimental conditions were pooled by sign inverting the turning response of the mirror-symmetrical condition. In (B), (C), and (D), n = 10 with 50 trials per fly; in (E), (F), (G), and (H), n = 10 with 40 trials per fly. In (H), the Wilcoxon rank-sum test was used to test for statistically significant differences. In (F), the Wilcoxon signed-rank test was performed. *$p < 0.05$. See also Figure S2.

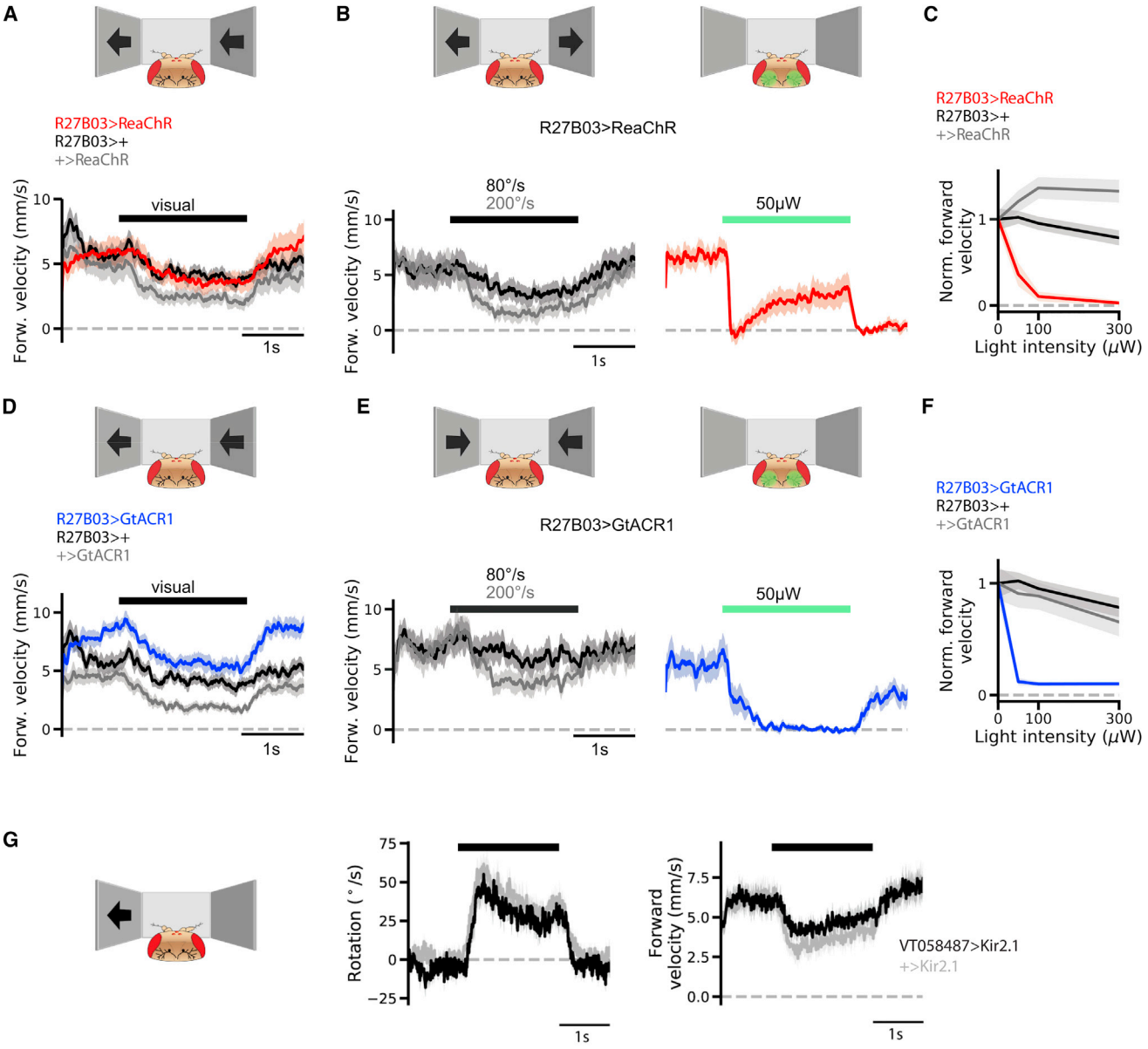

Figure 4. Control of Forward Walking Velocity and Requirement of HS Cells

(A) Forward walking response to binocular visual rotation stimulus (80°/s). Flies slow down during turning.

(B) Binocular visual stimulation (front-to-back motion with 80°/s in black and 200°/s in gray) in comparison with bilateral optogenetic HS cell depolarization.

(C) Quantification of bilateral optogenetic stimulation for R27B03 > ReaChR and controls. Hereby, the forward velocity of each genotype was normalized with respect to its average forward velocity in the dark.

(D) Experiment as described in (A), with partly different genotypes.

(E) Binocular visual HS cell hyperpolarization (back-to-front motion with 80°/s in black and 200°/s in gray) in comparison with bilateral optogenetic HS cell hyperpolarization.

(F) Quantification of bilateral optogenetic stimulation for R27B03 > GtACR1 and controls. The data have been normalized as explained in (C).

(G) Rotation and forward walking velocity in response to monocular front-to-back motion of control flies (+ > Kir2.1, gray) and flies with HS cells silenced by expression of the K^+-channel Kir2.1 (VT058487 > Kir2.1, black). Neither visual response component is clearly affected by HS cell silencing. Traces represent the mean ± SEM. Symmetric experimental conditions were pooled during analysis.

In (A) and (D), n = 10 with 40 trails per fly; in (B), (C), (E), and (F), n = 10 with 30 trails per fly. See also Figure S3.

new features: (1) according to their response sign, HS cells can signal two visual motion directions to downstream pathways and (2) these pathways have a predominantly negative effect on the propulsive forces underlying walking (Figure 1G).

Two Fundamental Functions of ND Input Integration

Motion opponency, i.e., the integration of excitatory PD and inhibitory ND responses, is a widespread phenomenon in wide-field motion-sensitive neurons in animals [30–33]. One

likely purpose is to ensure flow field selectivity. For instance, expanding flow impinges onto fly lobula plate tangential cells via retinotopically organized excitatory T4/T5 and inhibitory LPi connections in different parts of the dendrite. By spatial integration, responses cancel each other, thereby enhancing selectivity to unidirectional optic flow [19]. Furthermore, at least in flies, tangential cells are electrically coupled to each other, allowing transmission of de- and hyperpolarizations. Such coupling has been shown to support robust representation of optic flow parameters averaging out pattern-dependent modulations of local motion detector responses [34]. Here, we demonstrate an additional role of hyperpolarization in response to null direction motion as a direction-selective signal feeding into motor circuits that are involved in controlling heading.

Visually and Optogenetically Evoked Behavioral Responses

In tethered open loop behavior, locomotor responses to horizontal visual wide-field motion are well in line with HS cell activity mediating the behavior. For instance, unilateral motion evokes syndirectional turning, as is also the case for the equivalent optogenetically induced HS cell activity changes, implying a causal relationship (Figures 3B–3D). Regarding the influence of rotating and translating pattern motion on forward walking velocity, we see predominantly negative effects (Figure 4), in line with a previous study [27]. This negative effect is also apparent during bilaterally symmetric optogenetic HS cell stimulation, where flies slow down or stop. In extreme cases, walking velocity may even reverse. This suggests that turning is brought about predominantly by a negative effect—in part mediated by HS cells—on the propulsive forces underlying walking on the inner side of the curve. However, a positive influence on visually evoked walking responses has also been documented [13]. It therefore seems possible that the control system depicted in Figure 1G co-exists with alternative ones, which are differentially weighted depending on the experimental conditions. Although optogenetic HS cell manipulations recapitulate qualitative aspects of visually guided behavior, differences exist regarding the dynamics. For instance, horizontal motion evokes tonic responses both in HS cell activity and turning behavior. Optogenetic HS cell responses have a similar strong tonic component, yet turning behavior is more phasic in nature (Figures 2B, 2D, and 3B). This could indicate the existence of a control mechanism counteracting HS-cell-mediated responses in the absence of activity in other neurons that would normally occur during visual motion.

Requirement of HS Cells for Optomotor Turning

An important question pertains to the requirement of HS cells for optomotor turning. Before the advent of genetically targeted cell-specific manipulations in *Drosophila*, this had been attempted using mutant analysis and surgical interventions [35–37]. Perhaps the most selective manipulation has been conducted by severing the axons of HS cells unilaterally in tethered flying *Calliphora* [37]. This led to a reduction in optomotor turning in response to front-to-back motion on the lesioned side. The residual turning and the caveat that other cells were likely affected by the microsurgical procedures in the intricate network of motion-sensitive cells [38] suggests that other neurons apart from HS cells provide horizontal optic-flow-related information to downstream pathways. In agreement with this notion, in *Drosophila*, prolonged hyperpolarization of HS cells via expression of the K^+ channel Kir2.1 had only a subtle effect on visual-motion-evoked wing steering responses, with normal response amplitudes but a trend toward slower response acceleration at high visual motion speeds [16]. We have tested flies with the same manipulation in the tethered walking assay and did not find a consistent phenotype in the response amplitude or time course (Figures 4G and S3). The outcome that responses to monocular back-to-front and front-to-back motion remained intact further strengthens the conclusion that HS cells are part of a redundant system on each side of the head (Figures 1B, 1C, and 1G). One layer 2 candidate is the H2 cell [6]. Although H2 conveys motion information onto HS cell terminals via contralateral projections (a pathway removed by HS cell silencing) [39], H2 potentially provides synaptic input directly onto descending neurons, a pathway left intact by HS cell silencing. Another layer 2 candidate is the Hx cell [8, 9]. Furthermore, additional yet unidentified lobula plate layer 2 output neurons are likely to exist. The absence of a robust HS loss-of-function phenotype, as opposed to a 50% reduction suggested by the circuit depicted in Figure 1G, could be explained by a potentially saturated steering signal or homeostatic circuit compensation, due to a non-inducible prolonged silencing effect. Furthermore, the existence of other layer 1 output neurons underlying optomotor turning should not be excluded.

Downstream Pathways

Regarding how HS cell signals are conveyed to downstream motor centers, the schematic control circuit depicted in Figure 1G is clearly an oversimplification. For instance, it does not capture any lateral information transfer among tangential cells, which are conveyed via gap junctions or chemical synaptic connectivity, both ipsilaterally and across hemispheres [38, 39]. Any HS cell activity is thus expected to spread through the tangential cell network, likely to impinge on not just one but potentially several descending pathways in parallel. Although first steps have been made to identify those targets [40], many more descending neurons likely remain to be identified [41]. Furthermore, HS and other tangential cells provide input to neck motor neurons [15, 42], thereby likely controlling head movements following panoramic flow [16]. Leg and wing movements underlying steering might thus be implemented more indirectly via a control loop involving proprioceptive feedback from head posture. Despite the yet unknown intricacies, our data support the idea that de- and hyperpolarizing HS cell signals feed into at least two separate pathways. This is because both signals have a decelerating influence on the walking motor, which has to be exerted on opposite sides to support optomotor turning (Figure 1G).

Behavioral Significance of HS Cell Activity

Although it is becoming clear that HS cell activity influences locomotor behavior, the underlying biological significance is a different and more difficult question to address. Our results on asymmetric HS activity manipulations are consistent with the idea that HS cell activity represents an optic flow-based error signal related to self-rotation that counteracts unintended course deviations. However, vision is naturally implemented within action-perception feedback cycles imposing complex dynamics and involving rotational and translational motion

components. Two approaches have been taken in the past to capture naturalistic HS cell responses.

First, using sophisticated technology, the retinal input during unrestrained exploratory behavior of flying *Calliphora* has been reconstructed and HS cells' activity recorded during stimulus replay in order to determine which rotational and translational features they encode. It emerged that HS cell activity—in addition to rotational flow—is substantially modulated by translational motion, particularly in the slow response components. Because translational motion velocity depends on distance, HS activity may be implicated in obtaining spatial environmental information [1, 10, 11]. Indeed, fruit flies are well capable of using motion parallax cues for assessing distance [43–45]. The effect of artificial unilateral activation of HS cells may therefore additionally reflect naturally occurring attraction to a nearby surface or object. Perhaps related to that, binocular front-to-back motion leading to symmetric HS cell activation may indicate expansion as experienced on a collision course and require deceleration. The reverse scenario, binocular back-to-front motion leading to symmetric HS hyperpolarization, in particular during forward walking, may indicate a receding object, leading to deceleration as part of a freezing response [46].

As a second approach, tangential cell signals have been recorded during restrained walking and flight behavior. This showed that lobula plate tangential cells—in addition to visual input—integrate prominent internal motor-related signals. Those were shown to modulate response gain and speed tuning of HS cells [47, 48]. Strikingly, HS and other tangential cells also receive non-visual signals related to turning [14, 16, 49]. In tethered flight, those signals have appropriate signs to silence the expected visual reafference and are thus well suited to serve as efference copies. The remaining visual activity may therefore indicate accidental course deviations, useful for corrective steering [16, 49]. The situation in tethered walking flies is different. There, the visual reafference and non-visual turning signals have the same sign and therefore cooperate to produce larger direction-selective responses in HS cells during turns. Furthermore, HS cells receive depolarizing signals related to walking speed, in addition to the expected depolarizing visual reafference [14]. Why then does optogenetic but not self-generated HS cell activation lead to deceleration? This apparent paradox could be resolved by assuming a processing stage downstream of HS cells, where decelerating error signals are generated by subtracting an expected (via efference copy) from the actual (e.g. optogenetic) response.

Optic flow sensors are thus embedded in sophisticated state-dependent feedback systems, making it non-trivial to infer the role of HS cell activity during natural locomotion. However, as we have done here, an important step is to study the consequences of acute activity manipulations during visually guided behavior. Building on this study, careful analysis of other loss- and gain-of-function phenotypes during restrained and unrestrained behavior will provide further insights into optic-flow-based course control.

STAR★METHODS

Detailed methods are provided in the online version of this paper and include the following:

- KEY RESOURCES TABLE
- CONTACT FOR REAGENT AND RESOURCE SHARING
- EXPERIMENTAL MODEL AND SUBJECT DETAILS
  - Fly stocks
  - Detailed genotypes of flies used by figures
- METHOD DETAILS
  - Electrophysiology
  - Optomotor behavior assay setup
  - Optomotor behavior assay experiments
  - Blocking behavior assays
  - Confocal imaging
- QUANTIFICATION AND STATISTICAL ANALYSIS

SUPPLEMENTAL INFORMATION

Supplemental Information includes three figures and can be found with this article online at https://doi.org/10.1016/j.cub.2018.11.010.

ACKNOWLEDGMENTS

We are very grateful to Wolfgang Essbauer, Michael Sauter, Renate Gleich, Christian Theile, and Romina Kutlesa for excellent technical assistance. We would also like to thank Julia Kuhl for artwork. Fly lines were obtained from Bloomington, unless stated otherwise. We greatly appreciate helpful feedback on the manuscript from Aljoscha Leonhardt and Ines Ribeiro. Funding was provided from the Max Planck Society and the SFB 870 of the German Research Foundation.

AUTHOR CONTRIBUTIONS

Conceptualization, A.S.M., C.B., and A.B.; Methodology, A.S.M., C.B., and A.B.; Formal Analysis, A.S.M. and C.B.; Investigation, A.S.M. and C.B.; Writing – Original Draft, A.S.M.; Writing – Review & Editing, A.S.M., C.B., and A.B.; Supervision, A.S.M. and A.B.; Funding Acquisition, A.S.M. and A.B.

DECLARATION OF INTERESTS

The authors declare no competing interests.

Received: August 3, 2018
Revised: October 2, 2018
Accepted: November 2, 2018
Published: December 6, 2018

REFERENCES

1. Egelhaaf, M., Kern, R., and Lindemann, J.P. (2014). Motion as a source of environmental information: a fresh view on biological motion computation by insect brains. Front. Neural Circuits *8*, 127.
2. Borst, A. (2014). Fly visual course control: behaviour, algorithms and circuits. Nat. Rev. Neurosci. *15*, 590–599.
3. Mauss, A.S., and Borst, A. (2017). Motion vision in arthropods. In The Oxford Handbook of Invertebrate Neurobiology, J.H. Byrne, ed. (Oxford University Press).
4. Krapp, H.G. (2000). Neuronal matched filters for optic flow processing in flying insects. Int. Rev. Neurobiol. *44*, 93–120.
5. Krapp, H.G., and Wicklein, M. (2008). Central processing of visual information in insects. In The Senses: A Comprehensive Reference, Volume 1, R.H. Masland, T.D. Albright, P. Dallos, D. Oertel, S. Firestein, G.K. Beauchamp, M.C. Bushnell, A.I. Basbaum, J.H. Kaas, and E.P. Gardner, eds. (Academic Press), pp. 131–203.
6. Hausen, K. (1984). The lobula-complex of the fly: structure, function and significance in visual behaviour. In In Photoreception and Vision in Invertebrates, M.A. Ali, ed. (Springer), pp. 523–559.

7. Schnell, B., Joesch, M., Forstner, F., Raghu, S.V., Otsuna, H., Ito, K., Borst, A., and Reiff, D.F. (2010). Processing of horizontal optic flow in three visual interneurons of the *Drosophila* brain. J. Neurophysiol. *103*, 1646–1657.
8. Krapp, H.G., and Hengstenberg, R. (1996). Estimation of self-motion by optic flow processing in single visual interneurons. Nature *384*, 463–466.
9. Wasserman, S.M., Aptekar, J.W., Lu, P., Nguyen, J., Wang, A.L., Keleş, M.F., Grygoruk, A., Krantz, D.E., Larsen, C., and Frye, M.A. (2015). Olfactory neuromodulation of motion vision circuitry in *Drosophila*. Curr. Biol. *25*, 467–472.
10. Karmeier, K., van Hateren, J.H., Kern, R., and Egelhaaf, M. (2006). Encoding of naturalistic optic flow by a population of blowfly motion-sensitive neurons. J. Neurophysiol. *96*, 1602–1614.
11. Kern, R., van Hateren, J.H., Michaelis, C., Lindemann, J.P., and Egelhaaf, M. (2005). Function of a fly motion-sensitive neuron matches eye movements during free flight. PLoS Biol. *3*, e171.
12. Huston, S.J., and Krapp, H.G. (2008). Visuomotor transformation in the fly gaze stabilization system. PLoS Biol. *6*, e173.
13. Götz, K.G., and Wenking, H. (1973). Visual control of locomotion in the walking fruit fly *Drosophila*. J. Comp. Physiol. *85*, 235–266.
14. Fujiwara, T., Cruz, T.L., Bohnslav, J.P., and Chiappe, M.E. (2017). A faithful internal representation of walking movements in the *Drosophila* visual system. Nat. Neurosci. *20*, 72–81.
15. Haikala, V., Joesch, M., Borst, A., and Mauss, A.S. (2013). Optogenetic control of fly optomotor responses. J. Neurosci. *33*, 13927–13934.
16. Kim, A.J., Fenk, L.M., Lyu, C., and Maimon, G. (2017). Quantitative predictions orchestrate visual signaling in *Drosophila*. Cell *168*, 280–294.e12.
17. Mauss, A.S., Meier, M., Serbe, E., and Borst, A. (2014). Optogenetic and pharmacologic dissection of feedforward inhibition in *Drosophila* motion vision. J. Neurosci. *34*, 2254–2263.
18. Maisak, M.S., Haag, J., Ammer, G., Serbe, E., Meier, M., Leonhardt, A., Schilling, T., Bahl, A., Rubin, G.M., Nern, A., et al. (2013). A directional tuning map of *Drosophila* elementary motion detectors. Nature *500*, 212–216.
19. Mauss, A.S., Pankova, K., Arenz, A., Nern, A., Rubin, G.M., and Borst, A. (2015). Neural circuit to integrate opposing motions in the visual field. Cell *162*, 351–362.
20. Braitenberg, V. (1986). Vehicles: Experiments in Synthetic Psychology (MIT Press).
21. Buchner, E., Buchner, S., and Bülthoff, I. (1984). Deoxyglucose mapping of nervous activity induced in *Drosophila* brain by visual movement. J. Comp. Physiol. *155*, 471–483.
22. Inagaki, H.K., Jung, Y., Hoopfer, E.D., Wong, A.M., Mishra, N., Lin, J.Y., Tsien, R.Y., and Anderson, D.J. (2014). Optogenetic control of *Drosophila* using a red-shifted channelrhodopsin reveals experience-dependent influences on courtship. Nat. Methods *11*, 325–332.
23. Lin, J.Y., Knutsen, P.M., Muller, A., Kleinfeld, D., and Tsien, R.Y. (2013). ReaChR: a red-shifted variant of channelrhodopsin enables deep transcranial optogenetic excitation. Nat. Neurosci. *16*, 1499–1508.
24. Mauss, A.S., Busch, C., and Borst, A. (2017). Optogenetic neuronal silencing in *Drosophila* during visual processing. Sci. Rep. *7*, 13823.
25. Govorunova, E.G., Sineshchekov, O.A., Janz, R., Liu, X., and Spudich, J.L. (2015). NEUROSCIENCE. Natural light-gated anion channels: A family of microbial rhodopsins for advanced optogenetics. Science *349*, 647–650.
26. Jenett, A., Rubin, G.M., Ngo, T.-T.B., Shepherd, D., Murphy, C., Dionne, H., Pfeiffer, B.D., Cavallaro, A., Hall, D., Jeter, J., et al. (2012). A GAL4-driver line resource for *Drosophila* neurobiology. Cell Rep. *2*, 991–1001.
27. Silies, M., Gohl, D.M., Fisher, Y.E., Freifeld, L., Clark, D.A., and Clandinin, T.R. (2013). Modular use of peripheral input channels tunes motion-detecting circuitry. Neuron *79*, 111–127.
28. Mauss, A.S., Vlasits, A., Borst, A., and Feller, M. (2017). Visual circuits for direction selectivity. Annu. Rev. Neurosci. *40*, 211–230.
29. Borst, A., and Helmstaedter, M. (2015). Common circuit design in fly and mammalian motion vision. Nat. Neurosci. *18*, 1067–1076.
30. Wylie, D.R., Bischof, W.F., and Frost, B.J. (1998). Common reference frame for neural coding of translational and rotational optic flow. Nature *392*, 278–282.
31. Duffy, C.J., and Wurtz, R.H. (1991). Sensitivity of MST neurons to optic flow stimuli. I. A continuum of response selectivity to large-field stimuli. J. Neurophysiol. *65*, 1329–1345.
32. Ibbotson, M.R. (1991). Wide-field motion-sensitive neurons tuned to horizontal movement in the honeybee, *Apis mellifera*. J. Comp. Physiol. A *168*, 91–102.
33. Collett, T.S., and Blest, A.D. (1966). Binocular, directionally selective neurones, possibly involved in the optomotor response of insects. Nature *212*, 1330–1333.
34. Elyada, Y.M., Haag, J., and Borst, A. (2009). Different receptive fields in axons and dendrites underlie robust coding in motion-sensitive neurons. Nat. Neurosci. *12*, 327–332.
35. Heisenberg, M., Wonneberger, R., and Wolf, R. (1978). Optomotor-blind^{H31} – a *Drosophila* mutant of the lobula plate giant neurons. J. Comp. Physiol. *124*, 287–296.
36. Geiger, G., and Nässel, D.R. (1981). Visual orientation behaviour of flies after selective laser beam ablation of interneurones. Nature *293*, 398–399.
37. Hausen, K., and Wehrhahn, C. (1990). Neural circuits mediating visual flight control in flies. II. Separation of two control systems by microsurgical brain lesions. J. Neurosci. *10*, 351–360.
38. Borst, A., and Weber, F. (2011). Neural action fields for optic flow based navigation: a simulation study of the fly lobula plate network. PLoS ONE *6*, e16303.
39. Haag, J., and Borst, A. (2001). Recurrent network interactions underlying flow-field selectivity of visual interneurons. J. Neurosci. *21*, 5685–5692.
40. Suver, M.P., Huda, A., Iwasaki, N., Safarik, S., and Dickinson, M.H. (2016). An array of descending visual interneurons encoding self-motion in *Drosophila*. J. Neurosci. *36*, 11768–11780.
41. Namiki, S., Dickinson, M.H., Wong, A.M., Korff, W., and Card, G.M. (2018). The functional organization of descending sensory-motor pathways in *Drosophila*. eLife *7*, e10806.
42. Haag, J., Wertz, A., and Borst, A. (2010). Central gating of fly optomotor response. Proc. Natl. Acad. Sci. USA *107*, 20104–20109.
43. Cabrera, S., and Theobald, J.C. (2013). Flying fruit flies correct for visual sideslip depending on relative speed of forward optic flow. Front. Behav. Neurosci. *7*, 76.
44. Schuster, S., Strauss, R., and Götz, K.G. (2002). Virtual-reality techniques resolve the visual cues used by fruit flies to evaluate object distances. Curr. Biol. *12*, 1591–1594.
45. Pick, S., and Strauss, R. (2005). Goal-driven behavioral adaptations in gap-climbing *Drosophila*. Curr. Biol. *15*, 1473–1478.
46. Zabala, F., Polidoro, P., Robie, A., Branson, K., Perona, P., and Dickinson, M.H. (2012). A simple strategy for detecting moving objects during locomotion revealed by animal-robot interactions. Curr. Biol. *22*, 1344–1350.
47. Chiappe, M.E., Seelig, J.D., Reiser, M.B., and Jayaraman, V. (2010). Walking modulates speed sensitivity in *Drosophila* motion vision. Curr. Biol. *20*, 1470–1475.
48. Maimon, G., Straw, A.D., and Dickinson, M.H. (2010). Active flight increases the gain of visual motion processing in *Drosophila*. Nat. Neurosci. *13*, 393–399.
49. Kim, A.J., Fitzgerald, J.K., and Maimon, G. (2015). Cellular evidence for efference copy in *Drosophila* visuomotor processing. Nat. Neurosci. *18*, 1247–1255.
50. von Reyn, C.R., Breads, P., Peek, M.Y., Zheng, G.Z., Williamson, W.R., Yee, A.L., Leonardo, A., and Card, G.M. (2014). A spike-timing mechanism for action selection. Nat. Neurosci. *17*, 962–970.
51. Mauss, A.S., and Borst, A. (2016). Electrophysiological recordings from lobula plate tangential cells in *Drosophila*. Methods Mol. Biol. *1478*, 321–332.
52. Bahl, A., Ammer, G., Schilling, T., and Borst, A. (2013). Object tracking in motion-blind flies. Nat. Neurosci. *16*, 730–738.

STAR★METHODS

KEY RESOURCES TABLE

REAGENT or RESOURCE	SOURCE	IDENTIFIER
Chemicals, Peptides, and Recombinant Proteins		
all-trans retinal (ATR)	Sigma Aldrich	R2500
VECTASHIELD Antifade Mounting Medium	Vector Laboratories	Cat#H-1000; RRID: AB_2336789
Experimental Models: Organisms/Strains		
D. melanogaster: R27B03.Gal4^{attP2}	[47]	N/A
D. melanogaster: R24E09.Gal4^{attP2}	[16], BDSC	BDSC 49083
D. melanogaster: R81G07.Gal4^{attP2}	[14, 16], BDSC	BDSC 40122
D. melanogaster: VT023749.Gal4^{attP2}	[24]	N/A
D. melanogaster: VT058487.Gal4^{attP2}	[16]	N/A
D. melanogaster: tsh.Gal80	N/A	N/A
D. melanogaster: tub.Gal80-ts	Courtesy of Dana Galili & Hiromu Tanimoto	N/A
D. melanogaster: UAS.Kir2.1-GFP	Courtesy of Dana Galili & Hiromu Tanimoto	N/A
D. melanogaster: 10xUAS.Kir2.1-EGFP	[50]	N/A
D. melanogaster: UAS.mCD8-GFP on 2nd	Courtesy of T. Clandinin	N/A
D. melanogaster: UAS.GtACR1-EYFP^{attP40}	[24]	N/A
D. melanogaster: UAS.GtACR1-EYFP^{VK00005}	[24]	N/A
D. melanogaster: UAS.ReaChR-Citrine^{VK00005}	[22]	BDSC 53749
Software and Algorithms		
MATLAB (R2012b)	The MathWorks	RRID: SCR_001622
Python 3.5.2 (Anaconda)	Anaconda	https://www.anaconda.com
Fiji	NIH	RRID: SCR_002285
Other		
Sinfony Opaque Dentin (Near-ultraviolet bonding glue)	3M Espe	49530
BA OPTIMA 10	BA International	BASES10
Bridge amplifier	npi Electronics	BA-1S
Analog-to-digital converter	Measurement Computing	PCI-DAS6025
Wavelength switcher	Sutter Instrument Company	Lambda DG-4 Plus
Optical band-pass filter (Semrock 565/24 BrightLine HC)	AHF	F37-565
LED (565nm)	Thorlabs	M565F3
Fiber	Thorlabs	M15L01
Matched achromatic doublet pair	Thorlabs	MAP051950-A
Power energy meter	Thorlabs	PM100D
Rotary vane pump	Gardner Denver Thomas GmbH	G6/01-K-EB9L
High-power infrared LED (800nm)	Roithner Electronics	JET series, 90mW
Camera (fly positioning)	FLIR Integrated Imaging Solutions	CM3-U3-13S2M-CS
Monitor panel	BenQ	XL2411Z
Camera (optogenetic positioning)	FLIR Integrated Imaging Solutions	CM3-U3-13S2C-CS

CONTACT FOR REAGENT AND RESOURCE SHARING

Further information and requests for resources and reagents should be directed to and will be fulfilled by the Lead Contact, Alex S. Mauss (amauss@neuro.mpg.de).

EXPERIMENTAL MODEL AND SUBJECT DETAILS

Fly stocks

Flies were raised at 25°C and 60% humidity on standard cornmeal agar medium at a 12 h light/dark cycle. Experiment specific fly preparations and changes from the mentioned conditions are described in the corresponding method details sections. The following transgenic fly strains were used: R27B03.Gal4^{attP2} [47], R24E09.Gal4^{attP2} [16], R81G07.Gal4^{attP2} [14, 16], VT023749.Gal4^{attP2} [24], VT058487.Gal4^{attP2} [16], tsh.Gal80, tub.Gal80-ts and UAS.Kir2.1-GFP (courtesy of Dana Galili & Hiromu Tanimoto), 10xUAS.Kir2.1-EGFP [50], UAS.mCD8-GFP on 2nd (courtesy of T. Clandinin), UAS.GtACR1-EYFP^{attP40} [24], UAS.GtACR1-EYFP^{VK00005} [24], UAS.ReaChR-Citrine^{VK00005} [22].

Detailed genotypes of flies used by figures

Figure 2 and Figure S1

w+ ; UAS.mCD8-GFP/+ ; R27B03.Gal4/+
w+ ; + ; R27B03.Gal4/UAS.GtACR1-EYFP
w+ ; + ; R27B03.Gal4/UAS.ReaChR-Citrine

Figure 3

w+ ; + ; UAS.GtACR1-EYFP/+
w+ ; + ; UAS.ReaChR-Citrine/+
w+ ; + ; R27B03.Gal4/UAS.GtACR1-EYFP
w+ ; + ; R27B03.Gal4/UAS.ReaChR-Citrine
w+ ; + ; R27B03.Gal4/+
w+ ; + ; VT023749.Gal4/UAS.GtACR1-EYFP
w+ ; + ; VT023749.Gal4/UAS.ReaChR-Citrine
w+ ; tsh.Gal80/+ ; VT058487.Gal4/UAS.GtACR1-EYFP
w+ ; tsh.Gal80/+ ; VT058487.Gal4/UAS.ReaChR-Citrine
w+ ; UAS.GtACR1-EYFP ; R81G07.Gal4/UAS.GtACR1-EYFP
w+ ; + ; R81G07.Gal4/UAS.GtACR1-EYFP
w+ ; + ; R24E09.Gal4/UAS.GtACR1-EYFP
w+ ; + ; R24E09.Gal4/UAS.ReaChR-Citrine

Figure 4

w+ ; + ; UAS.GtACR1-EYFP/+
w+ ; + ; UAS.ReaChR-Citrine/+
w+ ; + ; R27B03.Gal4/UAS.GtACR1-EYFP
w+ ; + ; R27B03.Gal4/UAS.ReaChR-Citrine
w+ ; + ; R27B03.Gal4/+
w+ ; + ; 10xUAS.Kir2.1-EGFP/+
w+ ; tsh.Gal80/+ ; VT058487/10xUAS.Kir2.1-EGFP

Figure S2

w+ ; + ; R24E09.Gal4/UAS.GtACR1-EYFP
w+ ; + ; R27B03.Gal4/UAS.GtACR1-EYFP
w+ ; + ; R81G07.Gal4/UAS.GtACR1-EYFP
w+ ; UAS.GtACR1-EYFP ; R81G07.Gal4/UAS.GtACR1-EYFP
w+ ; + ; VT023749.Gal4/UAS.GtACR1-EYFP
w+ ; tsh.Gal80/+ ; VT058487.Gal4/UAS.GtACR1-EYFP

Figure S3

w+ ; + ; 10xUAS.Kir2.1-EGFP/+
w+ ; + ; R24E09/+
w+ ; + ; R24E09/10xUAS.Kir2.1-EGFP
w+ ; tsh.Gal80/+ ; VT058487/10xUAS.Kir2.1-EGFP
w+ ; + ; VT058487/10xUAS.Kir2.1-EGFP

w+ ; tub.Gal80-ts/+ ; R27B03.Gal4/UAS.Kir2.1-GFP
w+ ; tub.Gal80-ts/+ ; R81G07.Gal4/UAS.Kir2.1-GFP
w+ ; tub.Gal80-ts/+ ; VT023749.Gal4/UAS.Kir2.1-GFP

METHOD DETAILS

Electrophysiology

Fly preparation, whole-cell patch-clamp electrophysiology, visual and optogenetic stimulation and data acquisition were performed as described previously [51] and in the following sections. Experiments were performed at room temperature.

Fly preparation

All electrophysiological recordings were performed from 1-2 days old female flies. For optogenetic experiments, freshly eclosed flies were collected and transferred into a vial with yeast paste containing 1mM all-*trans*-retinal (ATR, R2500; Sigma Aldrich). Initially, flies were anesthetized on ice and attached to a custom holder made out of Plexiglas. The head was bend down and fixed in this position by attaching the proboscis to the ventral thorax using a droplet of melted beeswax. The holder was placed underneath a recording chamber with thin foil at the bottom, inserting the fly thorax into a 1 mm cutout, which also provided access to the back of the head. The remaining parts of the fly including the eyes remained below the edges of the cutout. The head was attached to the rim of the cutout using melted bees wax on one side. On the other side, using a hypodermic needle, a window was cut into the head capsule under external solution. Further steps were performed under a Zeiss Axiotech vario microscope which was equipped with polarized light contrast and epifluorescence. Using the polarized light and a cleaning micropipette with around 5 μm opening, a stream of 0.5 mg/ml Collagenase IV (GIBCO) was applied to digest the glia sheath locally.

Whole-cell recordings

Current-clamp recordings were performed with patch electrodes of 5-8 MΩ resistance. The signal was amplified, low pass filtered (3 kHz) and digitized with a sampling frequency of 10 kHz. The following hardware/software has been used: bridge amplifier (BA-1S, npi Electronics), analog-to-digital converter (PCI-DAS6025, Measurement Computing), MATLAB's data acquisition toolbox.

External and internal solutions

External solution contained the following (in mM): 103 *NaCl*, 3 *KCl*, 5 TES, 10 trehalose, 10 glucose, 7 sucrose, 26 $NaHCO_3$, 1 NaH_2PO_4, 1.5 $CaCl_2$, and 4 $MgCl_2$, pH 7.3–7.35, 280–290 mOsmol/kg. The external solution was carboxygenated (95% O_2/5% CO_2) and constantly perfused over the preparation at 2 ml/min. The internal solution, adjusted to pH 7.26 with 1N KOH, contained the following: 140 K-aspartate, 10 HEPES, 4 Mg-ATP, 0.5 Na-GTP, 1 EGTA, 1 KCl, and 0.1 Alexa Fluor 488 hydrazide salt (265 mOsmol/kg).

Visual stimulation

Visual stimulation was provided on a custom build LED arena (dimensions: 170° in azimuth and 90° in elevation) with the following properties: max. refresh rate of 600 Hz, max. luminance of 80 cd/m^2, spatial resolution of 1.4°.

Optogenetic stimulation

For optogenetic stimulation, light pulses were delivered by a Lambda DG-4 Plus wavelength switcher (Sutter Instrument) with a 300W Xenon Arc lamp via the epifluorescence light path of the microscope through a 40x/0.8 NA water-immersion objective (LUMPlan FI; Olympus). Light was passed through an optical filter with 565 nm center wavelength and 24 nm bandwidth (Semrock BrightLine HC). Intensities under the objective were measured with a power meter (Thorlabs PM100D) in air to estimate the irradiance per illuminated area in immersion.

Data analysis

For data representation, recording traces were averaged across trials and then cells to obtain the mean and standard deviation in MATLAB R2012b. For quantification, in each trial baseline and response was obtained by time-averaging the membrane potential 2 s before and after stimulus onset, respectively, and the baseline was then subtracted from the response. This value was then averaged across trials and cells. To obtain a measure for sensitivity of ReaChR and GtACR1, a sigmoid function of the form $y(x) = A/1 + e^{-k(x-x_0)}$ was fit to the data points as a function of light intensity x. A denotes the maximum response, k determines the steepness of the curve and x_0 indicates the x value of the curve midpoint. To obtain ON and OFF time constants τ, an exponential decay function of the form $y(t) = (N_0\text{-}N)e^{-t/\tau} + N$, with N_0 denoting the initial and N the final value, was fit to the light onset and offset responses as a function of time t. Curve fitting was done using the curve_fit tool from the scipy.optimize package in Python 3.5.2.

Optomotor behavior assay setup

In general, the experimental setup as well as the preparation used within this work are very similar to [24]. A full description of the fly preparation, tethering as well as the optogenetic and visual stimulation setup is provided in the following sections.

Fly preparation

Freshly hatched female flies were collected during one day. Within the same day, all collected flies were transferred into a vial with yeast-paste containing 1mM ATR. From here on, flies were kept at 25°C, 60% humidity on a 12h dark, 12h blue light cycle for two to three days, until the experiment was performed.

Tethering flies

The tethering procedure was performed while the fly was cooled down to 2°C, hence immobilized. Initially, the tip of a needle was positioned between head and thorax, whereby proper alignment of head and thorax was ensured. By doing so, the head was slightly tilted forward, allowing direct optogenetic stimulation of the back of the head during the experiments. Now, head, thorax and wings were tethered to the needle using near-ultraviolet bonding glue (Sinfony Opaque Dentin) and a blue LED light for drying (440 nm, BA OPTIMA 10, BA International).

Optogenetic stimulation

Unilateral as well as bilateral optogenetic stimulation were performed using the following setup – one for each side. The output of a fiber coupled LED of 565 nm wavelength (LED: M565F3 Thorlabs, Fiber: M15L01, Thorlabs) was focused onto a small point using a matched achromatic doublet pair (MAP051950-A, Thorlabs), which was connected to a micro-manipulator. The focused light point was around 0.12 mm^2 and could be precisely positioned onto the fly's head. Light intensities used within the experiments were calibrated with the help of a power energy meter (PM100D, Thorlabs).

Locomotion recorder

A locomotion recorder (as described in [52]) was used to record the waking behavior. It consists of an air-suspended polyurethane ball of 6 mm diameter floating in a bowl-shaped holder. The airflow, generated using a rotary vane pump (G6/01-K-EB9L, Gardner Denver Thomas GmbH), is adjusted in strength in such a way, that the ball is able to rotate freely inside the holder without jumping out. The ball is illuminated with the help of a high-power infrared LED (800 nm, JET series, 90mW, Roithner Electronics) and tracked using two optical tracking sensors. A camera (CM3-U3-13S2M-CS, FLIR Integrated Imaging Solutions) is positioned behind the ball in order to enable precise positioning of the fly on top of the ball. The positioning of the tethered fly is done using a micromanipulator.

Visual stimulation

Visual stimulation was provided using three 144 Hz monitor panels (XL2411Z, BenQ) covered with diffusion foil, which have been removed from their casing and vertically arranged into a U-shape. The luminance range of the covered panels ranges from 0 to 220 cd m^{-2}. The panel arrangement results in a visual arena with 30.5 × 33.5 × 56 cm, allowing to stimulate the fly's visual field within ± 135° horizontally and ± 61° vertically, with a pixel size smaller than 0.09°, whereby the fly was positioned in the center of the arena. All visual patterns were rendered on a virtual, upright cylinder surrounding the fly. Furthermore, an additional camera (CM3-U3-13S2C-CS, FLIR Integrated Imaging Solutions) was located over the fly in order to be able to position the optogenetic stimulation.

Optomotor behavior assay experiments

The following sections provide a detailed description of the optomotor behavior assay experiments. The temperature during all experiments was regulated to 34°C and the sequence of all tested conditions within each set was randomized. Flies which stopped walking before all experiments were performed were excluded from further analysis.

Unilateral optogenetic and visual stimulation

Each stimulus condition lasted five seconds. Unilateral optogenetic stimulation on the left or right side of the head started after one second and lasted two seconds long. Seven different LED intensities were tested (0.0 mW, 0.025 mW, 0.05 mW, 0.075 mW, 0.1 mW, 0.2 mW, 0.3 mW). Hereby, no visual stimulus was presented and the flies were in complete darkness. Visual responses were tested as follows. Initially, static vertical stripes with 10° width and random uniformly sampled intensity were presented only on the left or right side of the fly (+135° to +90° or −90° to −135° in azimuth). After one second, the visual pattern was moved for two seconds with an angular velocity of 80°/s clockwise or counter-clockwise. Subsequently, the pattern stayed one more second static before all monitors turned black.

Combined optogenetic and visual stimulation

Initially static vertical stripes with 10° width and random uniformly sampled intensity were presented only on the left or right side of the fly (+135° to +90° or −90° to −135° in azimuth). After one second, the visual pattern was moved for two seconds with an angular velocity of 80°/s clockwise or counter-clockwise. Simultaneously, the LED contralateral to the visual stimulus was turned on (intensities: 0.0 mW, 0.05 mW, 0.1 mW, 0.3 mW). After these two seconds, the LED turned off and the pattern stopped – being visible one more second before the screens turned black for six seconds.

Bilateral optogenetic or visual stimulation

Each bilateral stimulation condition lasted ten seconds. Optogenetic and visual stimulation were never combined. Bilateral optogenetic stimulation started after one second and lasted two seconds long. The following LED intensities for each channel were used: 0.0 mW, 0.05 mW, 0.1 mW, 0.3 mW. For bilateral visual stimulation, static vertical stripes with 10° width and random intensity taken from a uniform distribution were presented on the left and right side of the fly (+135° to +90° and −90° to −135° in azimuth). After one second, the visual patterns on both sides were rotated for two seconds simultaneously front-to-back or back-to-front (angular velocity of 80°/s or 200°/s). Again, the pattern motion stopped and one second later the screens were turned off.

Blocking behavior assays

The blocking behavior assays were performed on the same setup as the optomotor behavior assays.

Fly preparation and tethering

If possible, young, female flies were selected and kept on 25°C, 60% humidity on a 12h dark, 12h light cycle for two to three days, until the experiment was performed. However, some driver lines in combination with Kir were lethal. For those lines, tubGal80 was included to avoid expression during development. Now, young, female flies were selected and kept on 32°C, 60% humidity on a 12h dark, 12h light cycle for two to three days. The tethering procedure as well as the setup were identical to the optogenetic behavior assays. Again, the temperature during all experiments was set to 34°C and the sequence of all tested conditions within each set was randomized.

Visual stimulation

Each stimulus condition lasted five seconds. Initially static vertical stripes with 10° width and random uniformly sampled intensity were presented only on the left, right, left and right or all monitors of the setup (left: +135° to +90°, right: −90° to −135°, all: +135° to −135° in azimuth). Now, the visual pattern was moved for two seconds with an angular velocity of 80°/s clockwise or counter-clockwise. Subsequently, the pattern stopped, being visible for one more second, before all active screens turned black for one second.

Confocal imaging

Female flies (1-3 days old) were dissected in PBS and fixed at room temperature for 25min in PBS/4% paraformaldehyde (PFA). Subsequently they were washed in PBS and mounted using VECTASHIELD antifade mounting medium (Vector Laboratories). The expression pattern was optically sectioned using a Leica SP5 confocal scanning microscope. Hereby, confocal settings have not been altered between genotypes. Recorded stacks were processed using a maximum z-projection within Fiji.

QUANTIFICATION AND STATISTICAL ANALYSIS

Since experiments were performed and analyzed in a highly automated fashion, experimenters were not blinded to genotypes. Quantification and statistical analysis was performed using Python 3.5.2 (scipy.stats module). Information about the presented data, its quantification and statistical analysis are provided within the corresponding figure legends and within the figure. All behavioral tests were performed in a randomized order. In general, if not stated otherwise, traces represent mean over flies ± standard error of the mean (shaded envelope around trace or error bars). Behavioral traces were smoothed with a moving average of 50 ms. To test for significance, the data was first tested for normal distribution based on the skewness. For positive outcomes, the Wilcoxon rank-sum test was used to test for statistically significant differences. Otherwise, the Wilcoxon signed-rank test was used. Significance is indicated in figures with *, denoting $p < 0.05$.